

# SpectrumFM: A Foundation Model for Intelligent Spectrum Management

Fuhui Zhou, *Senior Member, IEEE*, Chunyu Liu, Hao Zhang, *Graduate Student Member, IEEE*, Wei Wu, *Member, IEEE*, Qihui Wu, *Fellow, IEEE*, Derrick Wing Kwan Ng, *Fellow, IEEE*, Tony Q. S. Quek, *Fellow, IEEE*, and Chan-Byoung Chae, *Fellow, IEEE*

**Abstract**—Intelligent spectrum management is crucial for improving spectrum efficiency and achieving secure utilization of spectrum resources. However, existing intelligent spectrum management methods, typically based on small-scale models, suffer from notable limitations in recognition accuracy, convergence speed, and generalization, particularly in the complex and dynamic spectrum environments. To address these challenges, this paper proposes a novel spectrum foundation model, termed SpectrumFM, establishing a new paradigm for spectrum management. SpectrumFM features an innovative encoder architecture that synergistically exploits the convolutional neural networks and the multi-head self-attention mechanisms to enhance feature extraction and enable robust representation learning. The model is pre-trained via two novel self-supervised learning tasks, namely masked reconstruction and next-slot signal prediction, which leverage large-scale in-phase and quadrature (IQ) data to achieve comprehensive and transferable spectrum representations. Furthermore, a parameter-efficient fine-tuning strategy is proposed to enable SpectrumFM to adapt to various downstream spectrum management tasks, including automatic modulation classification (AMC), wireless technology classification (WTC), spectrum sensing (SS), and anomaly detection (AD). Extensive experiments demonstrate that SpectrumFM achieves superior performance in terms of accuracy, robustness, adaptability, few-shot learning efficiency, and convergence speed, consistently outperforming conventional methods across multiple benchmarks. Specifically, SpectrumFM improves AMC accuracy by up to 12.1% and WTC accuracy by 9.3%, achieves an area under the curve (AUC) of 0.97 in SS at -4 dB signal-to-noise ratio (SNR), and enhances AD performance by over 10%.<sup>1</sup>

**Index Terms**—Spectrum foundation model, automatic modulation classification, wireless technology classification, spectrum sensing, anomaly detection.

F. Zhou is with the College of Artificial Intelligence and the Key Laboratory of Dynamic Cognitive System of Electromagnetic Spectrum Space, Nanjing University of Aeronautics and Astronautics, Nanjing 210000, China. (E-mail: {zhoufuhui@ieee.org})

C. Liu, H. Zhang, and Q. Wu are with the College of Electronic and Information Engineering, and with the Key Laboratory of Dynamic Cognitive System of Electromagnetic Spectrum Space, Nanjing University of Aeronautics and Astronautics, Nanjing 210000, China. (E-mail: {chunyu.liu@nuaa.edu.cn, haozhangcn@nuaa.edu.cn, wuqihui2014@sina.com})

W. Wu is with the College of Communication and Information Engineering, Nanjing University of Posts and Telecommunications, Nanjing 210003, China. (E-mail: {weiwu@njupt.edu.cn})

D. W. K. Ng is with the School of Electrical Engineering and Telecommunications, The University of New South Wales, Sydney, NSW 2052, Australia. (E-mail: {w.k.ng@unsw.edu.au})

T. Q. S. Quek is with the Singapore University of Technology and Design, Singapore 487372. (E-mail: {tonyquek@sutd.edu.sg})

C.-B. Chae is with the School of Integrated Technology, Yonsei University, Seoul 03722, South Korea. (E-mail: {cbchae@yonsei.ac.kr})

<sup>1</sup>The source code is available at <https://github.com/ChunyuLiu188/SpectrumFM.git>

## I. INTRODUCTION

THE radio frequency (RF) spectrum is a fundamental yet increasingly scarce resource in modern wireless communication networks [1]. As the demand for ubiquitous connectivity continues to rise, driven by the proliferation of Internet-of-Things (IoT) devices, non-terrestrial networks (NTNs), and the sixth-generation (6G) wireless paradigms, spectrum management is of crucial importance for improving spectrum efficiency, mitigating interference, detecting the illegal spectrum utilization, achieving reliable and secure spectrum operation [2], [3].

Spectrum management includes many tasks, such as spectrum sensing [4], spectrum analysis [5], spectrum resource decision-making [6], [7], etc. Intelligent spectrum management aims to exploit machine learning to achieve those tasks. The current intelligent spectrum management methods are mainly oriented for the specific task and only adapt to one task. Although those methods have achieved considerable success, they often exhibit limited generalization to unseen environments and require substantial amounts of labeled data for training. Moreover, their performance deteriorates in low signal-to-noise ratio (SNR) settings or under non-stationary signal conditions, which are prevalent in practical wireless environments.

Inspired by the transformative success of foundation models in natural language processing (e.g., BERT, GPT) and computer vision (e.g., ViT, Segment Anything), there is growing interest in developing foundation models for wireless communications [8], [9]. Those models are trained on large-scale heterogeneous data to learn universal representations that can be adapted to diverse downstream tasks with minimal supervision. Recent efforts, such as SpectralGPT [10] and Wireless-GPT [11], have demonstrated the potential of this paradigm in remote sensing and integrated sensing and communication (ISAC), respectively. However, the spectrum environment is inherently dynamic, with interference, signal fading, and noise introducing significant variability. This variability complicates the model ability to generalize across different environmental conditions and spectrum usage patterns. Moreover, the spectrum encompasses a broad range of frequency bands, from licensed to unlicensed, and the unpredictable nature of cognitive radio systems further amplifies the challenges. As a result, the application of foundation models to spectrum management remains largely unexplored.

To address this gap, we propose a novel spectrum founda-

tion model, termed SpectrumFM, a foundation model tailored for generalizable spectrum management across a wide range of tasks and environments. At its core, SpectrumFM employs a hybrid encoder architecture that exploits convolutional neural networks (CNNs) for localized feature extraction and multi-head self-attention (MHSA) modules for capturing long-range dependencies, enabling robust feature extraction and representation learning from large-scale in-phase and quadrature (IQ) data. Pre-training is conducted via two novel self-supervised learning tasks, namely masked reconstruction and next-slot signal prediction. The masked reconstruction task encourages the model to infer missing spectrum components, enhancing its ability to learn latent structures and intrinsic correlations while simultaneously improving its robustness to signal impairments such as noise and interference.

In contrast, the next-slot signal prediction task focuses on temporal continuity by training the model to anticipate future spectrum behavior, thereby improving its predictive capabilities and adaptability to the dynamic nature of the spectrum environment. Furthermore, efficient parameter fine-tuning allows SpectrumFM to generalize effectively across a wide range of downstream tasks, including automatic modulation classification (AMC), wireless technology classification (WTC), spectrum sensing (SS), and anomaly detection (AD). The main contributions of our work are summarized as follows.

- To the best of our knowledge, SpectrumFM is the first foundation model specifically designed for spectrum management, representing a promising new paradigm in this domain. In contrast to conventional methods that rely on hand-crafted features or task-specific architectures, SpectrumFM establishes an adaptable and highly generalizable framework capable of effectively addressing a wide range of spectrum-related tasks, including AMC, WTC, SS, and AD. Furthermore, it demonstrates strong robustness and adaptability across diverse environmental conditions and data distributions, effectively operating in real-world scenarios characterized by complex and dynamic spectrum data.
- SpectrumFM introduces a novel architectural and learning framework that significantly advances spectrum management by seamlessly exploiting CNNs and MHSA mechanisms to achieve an enhanced feature extraction from IQ signals. The CNN component excels at identifying fine-grained, localized spectral patterns, while the MHSA module models long-range dependencies, enabling the model to capture comprehensive, high-level representations of spectrum signals. To facilitate efficient pre-training without requiring extensive labeled data, we introduce two innovative self-supervised tasks, namely masked reconstruction and next-slot signal prediction. The masked reconstruction task enables the model to learn the underlying structure of the spectrum signals by predicting missing parts of the input, while the next-slot signal prediction task enhances the model temporal awareness by training it to predict future spectrum values based on historical data. As a result, these two

tasks allow SpectrumFM to develop rich and transferable representations that can generalize well across complex and dynamic spectrum environments.

- We conduct comprehensive experiments across four key downstream tasks, including AMC, WTC, SS, and AD, to rigorously evaluate the performance of our proposed model in comparison with state-of-the-art methods. The results highlight its effectiveness in diverse spectrum scenarios. Specifically, in the AMC task, SpectrumFM achieves notable accuracy improvements over existing methods, demonstrating enhanced robustness across datasets with varying complexities. In particular, it outperforms previous methods by 7.5% on the RML2016.10A dataset, 1.9% on the RML2016.10B dataset, and 12.1% on the RML2016.04C dataset. In the WTC task, our model exhibits a substantial classification accuracy gain, surpassing the best-performing baseline by 9.3%, highlighting its strong generalization ability in wireless technology identification. In the SS task, SpectrumFM achieves an area under the curve (AUC) of 0.97 even at a challenging SNR level of -4 dB, demonstrating exceptional robustness in low SNR environments. In the AD task, our model significantly enhances anomaly detection performance, achieving an AUC improvement of over 10%, underscoring its ability to identify complex spectrum anomalies with high precision. Overall, these results strongly validate the effectiveness, adaptability, and superior generalization ability of SpectrumFM across a wide range of spectrum management tasks.

The remainder of this paper is organized as follows. In Section II, we provide a comprehensive review of related works, focusing on task-specific spectrum management methods and recent advanced foundation models. Section III presents an in-depth description of our proposed SpectrumFM, detailing its architecture, design principles, and two novel pre-training tasks, namely mask reconstruction and next-slot signal prediction. Section IV outlines the experimental results obtained from evaluating our model on various downstream tasks. Finally, we conclude the paper in Section V, summarizing the key findings and discussing potential directions for future research.

## II. RELATED WORK

### A. Task-Specific Spectrum Management Methods

Spectrum management has traditionally been approached through task-specific methods, where models are designed and optimized for individual tasks such as AMC, WTC, SS, and AD. AMC, in particular, is a challenging task that requires accurate classification of the modulation scheme from a given IQ signal. Traditional methods have primarily relied on hand-crafted features, such as cyclic-moment-based features extracted through expert domain knowledge [12]. A significant milestone was achieved in [13], where CNNs were introduced to learn features automatically, eliminating the dependence on expert-designed representations. This marked the advent of deep learning techniques in AMC.

While CNNs demonstrated strong performance in extracting spatial features from IQ signals, they are inherently limited in modeling temporal dependencies. To address this, GrrNet [14] first employed a CNN-based module to extract representative features, followed by a gated recurrent unit (GRU) to capture temporal information. This hybrid design allowed GrrNet to balance spatial and temporal modeling, achieving notable improvements in AMC performance. However, GRUs still struggle with long-range dependencies and high-dimensional input data. To overcome these challenges, the authors in [15] proposed an attention-based AMC model. After initial feature extraction via a complex-valued CNN (CCNN), a modified multi-head attention mechanism was introduced, yielding a 1-10% accuracy improvement over GRU-based models.

Deep learning-based AMC methods often suffer from reliance on large amounts of labeled data. To mitigate this, SSwsrNet [16] introduced a semi-supervised learning framework based on MixMatch, effectively leveraging both labeled and unlabeled data. This method significantly enhanced performance in few-shot learning scenarios. In low SNR environments, AMC accuracy typically degrades due to noise interference. AMC\_Net [17] addressed this issue by applying signal denoising in the frequency domain, combined with multi-scale feature extraction. This approach significantly improved classification accuracy under low SNR conditions. However, denoising-based methods often rely on paired training data (i.e., clean and noisy signal pairs). To relax this constraint, [18] proposed a contrastive learning objective that eliminates the need for paired inputs. This method enhances generalization by enabling the model to learn from a broader distribution of signal variations across diverse noise conditions.

WTC is another challenging task that requires the model to accurately classify the type of wireless transmission based on the input IQ signal. Numerous studies have demonstrated significant progress in this area. For example, the authors in [19] employed CNNs to automatically extract features from the input signal and used a feedforward neural network to classify the wireless technology. Data augmentation techniques were also incorporated, enabling the model to generalize well to unseen scenarios while maintaining high accuracy. In [20], a multiscale module was introduced to capture features at various resolutions. Additionally, a global average pooling layer was utilized to aggregate the extracted features, which reduced the number of parameters and accelerated the training process. Despite its simplified architecture, the model achieved strong classification performance and fast convergence.

The authors in [21] proposed a comprehensive WTC system designed to identify and analyze a wide range of wireless technologies coexisting within the 5.9 GHz band. The system specifically focused on LTE, Wi-Fi, 5G NR, C-V2X PC5, and ITS-G5. To ensure accurate identification, the study adopted a short time resolution window based on the minimum frame duration of the target technologies. Unlike most IQ-based approaches, MFBLN [22] leveraged alternative features such as received signal strength indicator (RSSI), fast fourier transform (FFT), and spectrogram representations to extract multi-dimensional signal characteristics. This allowed the model to capture richer information from the input, thereby enhancing

classification accuracy and robustness across diverse wireless environments.

SS is a fundamental task in cognitive radio networks, referring to the process of monitoring and analyzing the RF spectrum to determine its occupancy status [23]. The primary goal of SS is to identify spectrum holes, which are unused or underutilized frequency bands in a specific geographical area. By detecting these holes, cognitive radios can dynamically access the available spectrum without interfering with primary users (PUs). SS is generally categorized into two types, namely narrowband SS and wideband SS. Narrowband SS analyzes one frequency band at a time, while wideband SS simultaneously evaluates multiple bands to identify vacant channels suitable for transmission [24]. Common narrowband SS techniques include energy detection, cyclostationary detection, and matched filter detection [25]. Among these, energy detection is widely used due to its simplicity. It determines spectrum occupancy by comparing the measured signal energy against a predefined threshold.

However, energy detection suffers from the well-known SNR wall issue caused by noise uncertainty, which significantly degrades its performance in low SNR environments. To address this limitation, the authors in [26] proposed a deep learning-based signal detector. Unlike conventional energy detection, the proposed method does not require prior knowledge of channel state information or background noise, resulting in greater robustness and adaptability under varying conditions. For wideband SS, the authors in [27] introduced a Transformer-based architecture that effectively learns both intra-band spectral features and inter-band occupancy correlations in the wideband regime. To further address the challenges of wideband SS under few-shot or cross-domain few-shot scenarios, the authors in [28] proposed a pre-training and fine-tuning approach leveraging transfer learning. This method improves performance when labeled data is scarce, making it well-suited for real-world applications where large annotated datasets are unavailable.

AD plays a critical role in enhancing spectrum sharing security, particularly in cognitive radio networks (CRNs) [29]. After spectrum sensing determines that the PU band is occupied, AD is employed to further assess whether the detected signal exhibits normal behavior or anomalous characteristics. The authors in [30] proposed an improved deep support vector data description (Deep SVDD) method for extracting low-dimensional features of the samples represented in the time-frequency domain. The method achieved excellent detection performance while maintaining real-time capability. To enable effective monitoring over a wide spectrum, a spectrum abnormal detection scheme was introduced in [31], which employed an adversarial autoencoder (AAE) to recover signals from sub-Nyquist samples. This design allowed for efficient processing of undersampled data while preserving the ability to detect spectral anomalies.

To address the challenge of implementing spectrum sensing and abnormal detection as separate modules, which increases system complexity and compromises real-time performance, the authors in [32] proposed a unified deep learning framework that performs spectrum sensing and abnormal detection simul-

taneously. This integrated approach delivers high detection accuracy while ensuring low-latency operation, offering a more efficient and practical solution for cognitive radio systems.

### B. Foundation Models

Foundation models are large-scale machine learning models that are pre-trained on vast amounts of data to learn general-purpose representations. The models serve as a foundational basis for a wide range of downstream tasks, making them highly versatile and adaptable across various domains. Foundation models are typically developed using deep learning techniques and are characterized by their massive scale, extensive training data, and strong transferability [33], [34]. The authors in [35] introduced the attention mechanism and the Transformer architecture, which serve as the cornerstone of foundation models. BERT [36] pioneered the era of foundation models. By introducing a bidirectional Transformer-based architecture and innovative pre-training strategies such as masked language modeling (MLM) and next sentence prediction (NSP), BERT achieved state-of-the-art performance on a wide range of natural language processing (NLP) tasks.

The BERT-like prediction loss is employed in HuBERT [37] for self-supervised speech representation learning, leading to the development of a speech foundation model. The authors in [38] present a foundational model that reformulates and unifies four core vision tasks, namely object detection, instance segmentation, keypoint prediction, and image captioning, into a single pixel-to-sequence framework. By framing multiple vision tasks within a shared pixel-to-sequence paradigm, this work demonstrated the potential of foundation models to generalize across tasks, reducing the need for specialized architectures and promoting greater flexibility in multimodal applications. SpectralGPT [10] represents a pioneering effort in creating a universal foundation model tailored for remote sensing (RS) applications. Trained on a large-scale dataset comprising one million spectral RS images, SpectralGPT achieved a parameter size exceeding 600 million. Evaluations across four downstream tasks reveal substantial performance improvements, highlighting the potential of foundation models to tackle a wide range of RS tasks.

WirelessGPT [11], a pioneering foundation model tailored for multi-task learning in ISAC, features an initial parameter size of approximately 80 million. Pre-trained on a large-scale wireless channel dataset, it delivers significant advancements in critical wireless tasks such as channel estimation, channel prediction, human activity recognition, and wireless reconstruction. WirelessGPT demonstrates that foundation models can achieve impressive performance improvements over conventional methods and smaller artificial intelligence (AI) models while requiring fewer labeled data, thereby enhancing efficiency and scalability in ISAC applications.

## III. OUR PROPOSED MODEL

In this section, we present our proposed foundational model for spectrum management. The overall framework of SpectrumFM is illustrated in Fig. 1, comprising three main stages,

TABLE I: Key Notations Used in the Paper.

Notation	Description
$\mathbf{x}_{ap}$	The AP signal.
$\mathbf{x}_{ap}^{norm}$	The normalized AP signal.
$abs(x)$	The amplitude function.
$angle(x)$	The phase function.
$p$	The position index.
$d$	The latent dimension.
$d_{feed}$	The feedforward dimension.
$i$	The index of the dimension.
$N$	The number of signal symbols.
$k$	The kernel size of the convolution layer.
$H$	The number of attention heads.
$h$	The attention head index.
$g$	The number of groups in the convolution layer.
$L$	The number of SpectrumFM encoder layers.
$\ell$	The SpectrumFM encoder layer index.
$r$	The mask ratio of signal symbols.
$\mathbf{m}$	The binary mask vector.
$\mathbf{M}$	The mask of attention scores.
$\Theta$	All the parameters of the SpectrumFM.
$E_p$	The number of epochs for pre-training.
$E_f$	The number of epochs for fine-tuning.
$\eta$	The learning rate.

namely, data collection and processing, pre-training, and fine-tuning. In the data collection and processing stage, we aggregate a comprehensive dataset from diverse sources, including publicly available open-source datasets and signals collected in real-world practice scenarios. A crucial aspect of this stage is data preprocessing, where normalization techniques are exploited to ensure seamless integration of heterogeneous data into a unified training framework. Furthermore, during the pre-training stage, SpectrumFM undergoes self-supervised learning on the integrated dataset exploiting two designed tasks, namely masked reconstruction and next-slot signal prediction. The two tasks enable the model to learn fundamental representations of spectrum data, capturing both generalizable patterns and environment-specific variations. Finally, in the fine-tuning stage, the pre-trained model is adapted to specific downstream tasks, including AMC, WTC, SS, and AD. The step ensures that SpectrumFM effectively captures task-specific spectrum features, enhancing its adaptability across diverse spectrum management applications. The variables used throughout this paper are summarized in TABLE I.

### A. Data Collection And Processing Stage

In the data collection and processing stage, a diverse set of spectrum data is gathered from multiple sources, including publicly available open-source datasets and signals collected in real-world for this study, to facilitate comprehensive training of SpectrumFM. The open-source datasets utilized in this study include the RML2018.01A dataset [39] and the technology recognition (TechRec) dataset<sup>2</sup>. The RML2018.01A dataset comprises 24 distinct modulation types, including OOK, 4-ASK, 8-ASK, BPSK, QPSK, 8-PSK, 16-PSK, 32-PSK, 16-APSK, 32-APSK, 64-APSK, 128-APSK, 16-QAM, 32-QAM, 64-QAM, 128-QAM, 256-QAM, AM-SSB-WC, AM-SSB-SC, AM-DSB-WC, AM-DSB-SC, FM, GMSK, and OQPSK.

<sup>2</sup><https://ieee-dataport.org/documents/iq-signals-captured-lte-wifi-and-dvb-t>

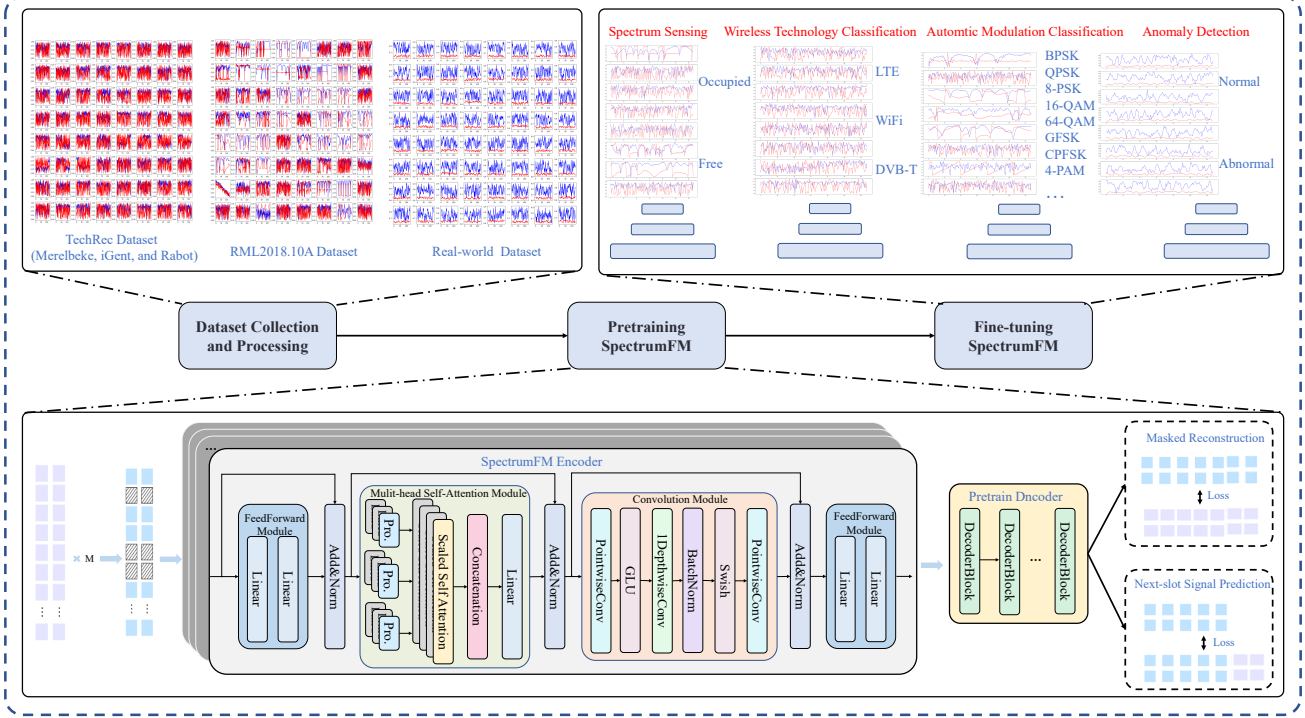


Fig. 1: The SpectrumFM framework comprises three key stages. First, in the data collection and processing stage, diverse spectrum data from multiple sources are gathered and preprocessed to ensure consistency and compatibility across datasets. Second, during the pre-training stage, the model learns fundamental spectrum representations through self-supervised learning tasks, namely, masked reconstruction and next-slot signal prediction. Finally, in the fine-tuning stage, the pre-trained model is adapted to specific downstream tasks, including AMC, WTC, SS, and AD.

This dataset spans a broad range of SNRs, ranging from -20 dB to 30 dB in increments of 2 dB, providing a comprehensive representation of diverse signal conditions. The TechRec dataset consists of over-the-air IQ samples collected from six distinct locations in Gent, Belgium, including UZ, Reep, Rabot, Merelbeke, iGent, and Gentbrugge. Each location exhibits unique signal characteristics due to variations in signal strength, noise levels, and physical propagation conditions. The SNR in the dataset ranges from -6 dB to 12 dB, with increments of 2 dB. Specifically, IQ samples collected from Merelbeke, iGent, and Rabot are leveraged for pre-training, while data from UZ, Reep, and Gentbrugge are exploited for fine-tuning and testing. In addition to the publicly available datasets, signals are also collected by using a ceyear 1435B-V RF signal generator for transmission and a SAM 60 MK2 receiver for reception. The total size of the pre-training dataset amounts to approximately 25 GB. The received signal  $H$  is formulated as

$$H : x(n) = f(s(n), F) + \omega(n), n = 1, 2, 3, \dots, N, \quad (1)$$

where  $x(n)$  and  $s(n)$  are the received signal and the transmitted signal, respectively,  $F$  represents the channel fading coefficient,  $N$  is the number of signal symbols, and  $\omega(n)$  is the additive white Gaussian noise with zero mean and variance  $\sigma^2$ . The IQ signal samples can be represented as a vector by transforming the received signal  $x(n)$  into the vector  $\mathbf{x}$ , given

as

$$\mathbf{x} = \mathbf{I} + \mathbf{Q}, \quad (2a)$$

$$= \Re(x) + j\Im(x), \quad (2b)$$

where  $\mathbf{I}$  and  $\mathbf{Q}$  represent the in-phase and quadrature components of the received signal, respectively, and  $j = \sqrt{-1}$ , and  $\Re(x)$  and  $\Im(x)$  correspond to the real and imaginary parts of the signal, respectively. The raw data  $\mathbf{x}$  can be explicitly represented in matrix form, given as

$$\mathbf{x} = \begin{bmatrix} \Re[x(1), x(2), \dots, x(N)] \\ \Im[x(1), x(2), \dots, x(N)] \end{bmatrix}. \quad (3)$$

To facilitate normalization, we first convert the IQ signals into amplitude-phase (AP) signals, since the value ranges of amplitude and phase components are better suited for standardization, specifically  $[-\pi, \pi]$  for the phase component and  $[0, +\infty]$  for the amplitude component. Mathematically, this transformation for the IQ signals to AP signals can be expressed as

$$\mathbf{x}_{ap} = \mathbf{A} \exp(j\Theta), \quad (4)$$

where  $\mathbf{A}$  is the amplitude component and  $\Theta$  is the phase component, respectively. It can be further expressed as

$$\mathbf{x}_{ap} = \begin{bmatrix} \text{abs}[x(1), x(2), \dots, x(N)] \\ \text{angle}[x(1), x(2), \dots, x(N)] \end{bmatrix}, \quad (5)$$

where  $\text{abs}[\cdot]$  and  $\text{angle}[\cdot]$  are the amplitude and phase functions, respectively, given as

$$\text{abs}(x) = \sqrt{\Re^2(x) + \Im^2(x)}, \quad (6a)$$

$$\text{angle}(x) = \arctan\left(\frac{\Im(x)}{\Re(x)}\right). \quad (6b)$$

To ensure that the distribution of each sample in different dataset is consistent while preserving the intrinsic characteristics of the data, we propose a sample-level normalization method, where each sample is normalized independently based on its own maximum and minimum values by using min-max normalization, given as

$$\mathbf{x}_{\text{ap}}^{\text{norm}} = \frac{x_{\text{ap}} - \min(x_{\text{ap}})}{\max(x_{\text{ap}}) - \min(x_{\text{ap}})}, \quad (7)$$

where  $\min(\cdot)$  and  $\max(\cdot)$  are the functions to obtain the minimum and maximum values of the sample  $x_{\text{ap}}$ , respectively.

### B. SpectrumFM Encoder

After obtaining the processed signal  $\mathbf{x}_{\text{ap}}^{\text{norm}}$ , a 1D convolution projection layer with a kernel size  $k = 1$  is leveraged to project the input signal into a higher-dimensional space, given as

$$\mathbf{x}_{\text{proj}}[p, :] = \sum_{c=0}^1 \mathbf{x}_{\text{ap}}^{\text{norm}}[p, c] \cdot \mathbf{W}_{\text{proj}}[0, c, :], \quad (8)$$

where  $\mathbf{x}_{\text{proj}} \in \mathbb{R}^{N \times d}$  is the projected signal,  $\mathbf{W}_{\text{proj}} \in \mathbb{R}^{d \times 2 \times 1}$  is the convolution kernel,  $d$  is the latent dimension, and  $p$  represents the position index, ranging from 0 to  $N - 1$ . To capture the sequential order in a signal sequence, positional encoding is added to  $\mathbf{x}_{\text{proj}}$ . The positional encoding is given as

$$\text{PE}_{p,2i} = \sin\left(\frac{p}{10000^{2i/d}}\right), \quad (9a)$$

$$\text{PE}_{p,2i+1} = \cos\left(\frac{p}{10000^{2i/d}}\right), \quad (9b)$$

where  $i$  is the index of the dimension, ranging from 0 to  $d - 1$ . The signal with the positional encoding is given as

$$\mathbf{x}_{\text{position}}[p, :] = \mathbf{x}_{\text{proj}}[p, :] + \text{PE}[p, :]. \quad (10)$$

Subsequently, the position-encoded signal  $\mathbf{x}_{\text{position}}$  is fed into the proposed SpectrumFM encoder to facilitate feature extraction. The SpectrumFM encoder follows a structured pipeline comprising an initial feedforward module, followed by a multi-head self-attention module, then a convolution module, and finally another feedforward module. Each module is connected with residual connections followed by normalization to stabilize the training process. This design is particularly well-suited for wireless communication applications, where spectrum management requires efficient feature extraction, robust signal representation, and adaptive processing. The feedforward module captures low-level signal characteristics, while multi-head self-attention models spectral dependencies, enhancing feature discernment in dynamic environments. Convolutions refine local spectral details, improving resilience to distortions, and the final feedforward module consolidates learned representations. Residual connections and normalization stabilize training, ensuring effective feature propagation.

Initially, the input sequence undergoes preliminary processing through an initial feedforward module, which enriches the feature representation by applying non-linear transformations. Specifically, the feedforward module consists of two linear transformations separated by a non-linear activation function. The output of the module can be expressed as

$$\mathbf{x}_{\text{ffn}} = RN(GELU(\mathbf{x}_{\text{position}} \mathbf{W}_1 + \mathbf{b}_1) \mathbf{W}_2 + \mathbf{b}_2), \quad (11)$$

where  $\mathbf{W}_1 \in \mathbb{R}^{d \times d_{\text{feed}}}$  and  $\mathbf{W}_2 \in \mathbb{R}^{d_{\text{feed}} \times d}$  are the weight matrices,  $\mathbf{b}_1 \in \mathbb{R}^{d_{\text{feed}}}$  and  $\mathbf{b}_2 \in \mathbb{R}^d$  are the bias vectors,  $d_{\text{feed}}$  is the feedforward dimension,  $GELU$  is the Gaussian error linear unit (GELU) activation function and  $RN$  represents the residual connection and normalization operation.

The enriched representation  $\mathbf{x}_{\text{ffn}}$  is then subjected to global dependency analysis via the multi-head self-attention mechanism, thereby enabling the model to capture long-range dependencies across the entire sequence. For each attention head  $h$ , the input  $\mathbf{x}_{\text{ffn}} \in \mathbb{R}^{N \times d}$  is transformed into query ( $\mathbf{Q}$ ), key ( $\mathbf{K}$ ), and value ( $\mathbf{V}$ ) matrices by using learnable weight matrices, given as

$$\mathbf{Q}_h = \mathbf{x}_{\text{ffn}} \mathbf{W}_Q^h, \quad (12a)$$

$$\mathbf{K}_h = \mathbf{x}_{\text{ffn}} \mathbf{W}_K^h, \quad (12b)$$

$$\mathbf{V}_h = \mathbf{x}_{\text{ffn}} \mathbf{W}_V^h, \quad (12c)$$

where  $\mathbf{W}_Q^h \in \mathbb{R}^{d \times d_h}$ ,  $\mathbf{W}_K^h \in \mathbb{R}^{d \times d_h}$ , and  $\mathbf{W}_V^h \in \mathbb{R}^{d \times d_h}$  are the learnable weight matrices,  $d_h = \frac{d}{H}$  denoting dimension of each head, and  $H$  is the number of heads. The output of each head  $h$  is computed by using a scaled dot-product attention, given as

$$\mathbf{x}_h = \text{softmax}\left(\frac{\mathbf{Q}_h \mathbf{K}_h^T}{\sqrt{d_h}}\right) \mathbf{V}_h, \quad (13)$$

where  $\text{softmax}(\cdot)$  applies the softmax function row-wise. The outputs from all heads are concatenated and linearly transformed to produce the final output of the multi-head self-attention module, given as

$$\mathbf{x}_{\text{attention}} = RN(\text{concat}(\mathbf{x}_1, \dots, \mathbf{x}_H) \mathbf{W}^o), \quad (14)$$

where  $\text{concat}(\cdot)$  is the concatenation operator, and  $\mathbf{W}^o \in \mathbb{R}^{d \times d}$  is the weight matrix.

Following the multi-head self attention module, the convolution module identifies and extracts local dependencies within localized regions of the sequence, enhancing the model ability to detect fine-grained patterns. Specifically, a 1D convolution layer with a kernel size  $k = 1$  and a gated linear unit (GLU) activation function is applied to the output of the multi-head self-attention module, given as

$$\mathbf{x}_{\text{inconv}}[p, :] = GLU\left(\sum_{c=0}^1 \mathbf{x}_{\text{attention}}[p, c] \cdot \mathbf{W}_{k1}[0, c, :]\right), \quad (15)$$

where  $\mathbf{W}_{k1} \in \mathbb{R}^{2d \times d \times 1}$  is the convolution kernel. And then, a 1D convolution layer with a kernel size  $k = 3$ , groups  $g = d$

and a swish activation function is leveraged to extract local dependencies, given as

$$\mathbf{x}_{\text{localconv}}[p, :] = \text{swish} \left( \sum_{c=0}^{d-1} \left( \underbrace{\mathbf{x}_{\text{inconv}}[p-1 : p+1, c]}_{\text{kernel size}=3} * \mathbf{W}_{k2}[c, :] \right) + \mathbf{b}_{k2} \right), \quad (16)$$

where  $\text{swish}(\cdot)$  represents the swish activation function,  $\mathbf{W}_{k2} \in \mathbb{R}^{d \times 1 \times 3}$  is the convolution kernel, and  $\mathbf{b}_{k2} \in \mathbb{R}^d$  is the bias. Another 1D convolution layer with kernel size  $k = 1$  is leveraged to further refine the extracted local features, given as

$$\mathbf{x}_{\text{outconv}}[p, :] = RN \left( \sum_{c=0}^1 \mathbf{x}_{\text{localconv}}[p, c] \cdot \mathbf{W}_{k3}[0, c, :] \right), \quad (17)$$

where  $\mathbf{W}_{k3} \in \mathbb{R}^{d \times d \times 1}$  is the convolution kernel.

Finally, a subsequent feedforward module integrates the insights obtained from both the attention and convolution modules, given as

$$\mathbf{x}_{\text{latent}} = (GELU(\mathbf{x}_{\text{outconv}} \mathbf{W}_3 + \mathbf{b}_3)) \mathbf{W}_4 + \mathbf{b}_4, \quad (18)$$

where  $\mathbf{W}_3 \in \mathbb{R}^{d \times d_{\text{feed}}}$  and  $\mathbf{W}_4 \in \mathbb{R}^{d_{\text{feed}} \times d}$  are the weight matrices,  $\mathbf{b}_3 \in \mathbb{R}^{d_{\text{feed}}}$  and  $\mathbf{b}_4 \in \mathbb{R}^d$  are the bias vectors.

To enhance the model representational capacity and capture more complex patterns within the input data, a multi-layer encoder architecture is exploited. Specifically, each layer of the encoder progressively transforms the latent representation from the previous layer until the  $L$ -th layer. The process can be expressed as

$$\mathbf{x}_{\text{latent}}^{(\ell)} = \text{encoder}(\mathbf{x}_{\text{latent}}^{(\ell-1)}), \quad (19)$$

where  $\text{encoder}(\cdot)$  is the SpectrumFM encoder,  $\mathbf{x}_{\text{latent}}^{(\ell)}$  is the latent representation of the  $\ell$ -th layer, and  $\mathbf{x}_{\text{latent}}^{(\ell-1)}$  is the latent representation of the previous layer. And the final output after  $L$  layers of the encoder is denoted as  $\mathbf{x}_{\text{latent}}^{(L)}$ .

### C. Pre-training Stage

To pre-train SpectrumFM without labeled data, two self-supervised pre-training tasks, namely mask reconstruction and next-slot signal prediction are proposed. These tasks are well-suited for spectrum data due to the dynamic and noisy nature of spectrum environments. Mask reconstruction helps the model learn robust signal representations by reconstructing missing or degraded signal segments, simulating real-world scenarios where signals are often impaired by noise and interference. Next-slot signal prediction is crucial for understanding the dynamic nature of spectrum usage. As the spectrum environment continuously evolves, predicting future spectrum behavior enables the model to adapt to these changes, ensuring effective management of the constantly shifting spectrum. As a result, these tasks enable SpectrumFM to learn the key characteristics of spectrum data, preparing it for real-world spectrum management challenges.

*1) The Masked Reconstruction Task:* In the masked reconstruction task, the objective is to mask a portion of the original AP sequence  $\mathbf{x}_{\text{ap}}^{\text{norm}}$  and train the model to reconstruct the masked parts. The task facilitates to learn general representations in an unsupervised manner by training the model to infer and reconstruct masked portions of the input data, thereby enhancing its robustness and generalization capabilities. Specifically, given the sequence  $\mathbf{x}_{\text{ap}}^{\text{norm}}$ , we first randomly mask a subset of the sequence according to a predefined masking ratio  $r$ . The binary mask vector  $\mathbf{m}$  is defined as  $\mathbf{m} \sim \text{Bernoulli}(1-r)$ , which consists of elements  $\{m_1, m_2, \dots, m_N\}$ . Here  $m_p = 0$  if the  $p$ -th symbol is masked out, and  $m_p = 1$  otherwise. The masked sequence is then given as

$$\mathbf{x}_{\text{ap}}^{\text{mask}} = \mathbf{x}_{\text{ap}}^{\text{norm}} \odot \mathbf{m}, \quad (20)$$

where  $\odot$  represents the element-wise multiplication. The masked AP sequence is then fed into the SpectrumFM encoders to obtain  $\mathbf{x}_{\text{latent}}^{(L)}$ . It is important to note that an attention mask  $\mathbf{M}$  is also applied during the computation of attention weights in the SpectrumFM encoders. Specifically, in the pre-training phase, equation (13) is updated as

$$\mathbf{x}_h = \text{softmax} \left( \frac{\mathbf{Q}_h \mathbf{K}_h^T}{\sqrt{d_h}} + \mathbf{M} \right) \mathbf{V}_h, \quad (21)$$

where  $\mathbf{M}$  assigns extremely small values (e.g.,  $-\infty$ ) to the positions that are masked out, thereby ensuring that the positions do not contribute to the computed attention weights. After obtaining  $\mathbf{x}_{\text{latent}}^{(L)}$ , a lightweight decoder is applied to the latent representation to reconstruct the original input sequence, given as

$$\mathbf{x}_{\text{recon}} = \mathbf{x}_{\text{latent}}^{(L)} \mathbf{W}_{\text{recon}} + \mathbf{b}_{\text{recon}}, \quad (22)$$

where  $\mathbf{W}_{\text{recon}} \in \mathbb{R}^{d \times 2}$  and  $\mathbf{b}_{\text{recon}} \in \mathbb{R}^2$  are the learnable weights and biases of the decoder, respectively. Finally, the mean squared error (MSE) loss is calculated by comparing the reconstructed sequence with the original input sequence in the masked region, given as

$$\mathcal{L}_{\text{recon}} = \frac{1}{\sum_{p=1}^N (1 - m_p)} \sum_{i=p}^N (1 - m_p) (\mathbf{x}_{\text{ap}}^{\text{norm}} - \mathbf{x}_{\text{recon}})^2. \quad (23)$$

*2) Next-slot Signal Prediction Task:* The next-slot signal prediction task aims to predict the signal symbol at the  $N$ -th time slot based on the historical signal observations from the previous  $N-1$  slots. The task facilitates SpectrumFM to understand the temporal characteristics of signals. Specifically,  $\mathbf{x}_{\text{ap}}^{\text{norm}}[:N-1]$  is input to the SpectrumFM encoders to obtain the latent representation  $\mathbf{x}_{\text{latent}}^{(L)}$ , and then an long short-term memory (LSTM) layer is leveraged to aggregate the latent representation, and finally a linear layer is exploited to predict the  $N$ -th signal symbol. Mathematically, the predicted signal symbol is given as

$$\hat{x}_{\text{ap}}^{\text{norm}}[N] = \sigma \left( \text{LSTM} \left( \mathbf{x}_{\text{latent}}^{(L)} \right) \mathbf{W}_{\text{pre}} + \mathbf{b}_{\text{pre}} \right), \quad (24)$$

where  $\sigma(\cdot)$  is the sigmoid function,  $\mathbf{W}_{\text{pre}} \in \mathbb{R}^{d \times 2}$  and  $\mathbf{b}_{\text{pre}} \in \mathbb{R}^2$  are the weights and biases of the linear layer, respectively. The MSE loss is adopted to train the task, given as

$$\mathcal{L}_{\text{pre}} = \frac{1}{2} (\hat{x}_{\text{ap}}^{\text{norm}}[N] - x_{\text{ap}}^{\text{norm}}[N])^2. \quad (25)$$

The Pre-training algorithm is summarized in Algorithm 1.

---

**Algorithm 1:** Pre-training Algorithm For SpectrumFM

---

**Input:** Pre-training dataset  
**Output:** All the parameters  $\Theta$  of SpectrumFM

- 1 Initialize all the parameters  $\Theta$  of SpectrumFM;
- 2 Set  $\text{best\_val\_loss} \leftarrow \infty$ ;
- 3 Set  $\text{no\_improvement\_count} \leftarrow 0$ ;
- 4 **for**  $\text{epoch} = 1$  to  $E_p$  **do**
- 5     **for** *batch data in the pretraining dataset* **do**
- 6         Preprocess the batch data according to equations (1) to (7);
- 7         Feed processed data into SpectrumFM encoders and obtain the latent representation  $\mathbf{x}_{\text{latent}}^{(L)}$  according to equations (8) to (19);
- 8         Obtain reconstructed signal symbols according to equations (20) to (22);
- 9         Compute reconstruction loss  $\mathcal{L}_{\text{recon}}$  according to equation (23);
- 10         Predict next-slot signal symbols according to equation (24);
- 11         Compute predicted loss  $\mathcal{L}_{\text{pre}}$  according to equation (25);
- 12         Obtain pre-training loss according to  $\mathcal{L} \leftarrow \alpha \mathcal{L}_{\text{recon}} + \beta \mathcal{L}_{\text{pre}}$ ;
- 13         Update  $\Theta$  using the pre-training loss according to  $\Theta \leftarrow \Theta - \eta \nabla_{\Theta} \mathcal{L}$ ;
- 14     **end**
- 15     Evaluate the model on the validation set and compute  $\text{val\_loss}$ ;
- 16     **if**  $\text{val\_loss} < \text{best\_val\_loss}$  **then**
- 17          $\text{best\_val\_loss} \leftarrow \text{val\_loss}$ ;
- 18          $\text{no\_improvement\_count} \leftarrow 0$ ;
- 19     **end**
- 20     **else**
- 21          $\text{no\_improvement\_count} \leftarrow \text{no\_improvement\_count} + 1$ ;
- 22     **end**
- 23     **if**  $\text{no\_improvement\_count} \geq 2$  **then**
- 24         **break**;
- 25     **end**
- 26 **end**
- 27 Return the pretrained parameters  $\Theta$ ;

---

#### D. Fine-tuning Stage

After completing the pre-training stage, which enables the model to acquire generalizable representations from large volumes of unlabeled data, the next critical step is the fine-tuning stage. During this phase, the pre-trained model is further refined for a specific downstream task exploiting a small but

---

**Algorithm 2:** Fine-tuning Algorithm For SpectrumFM

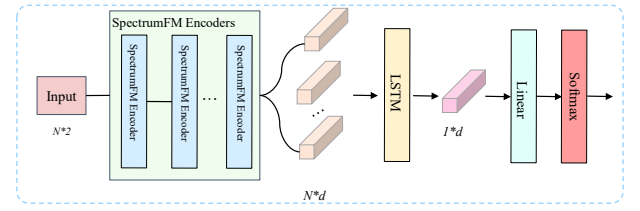
---

**Input:** Fine-tuning dataset, pre-trained parameters  $\Theta$   
**Output:** All the fine-tuned parameters  $\Theta$  of SpectrumFM

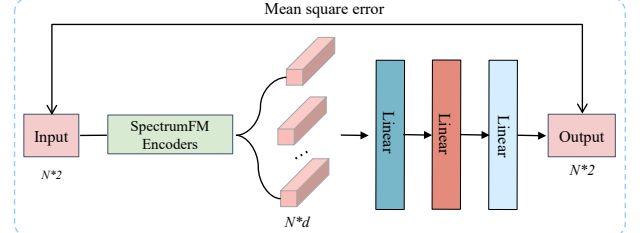
- 1 **for**  $\text{epoch} = 1$  to  $E_f$  **do**
- 2     **for** *batch data in the fine-tuning dataset* **do**
- 3         Preprocess the batch data according to equations (1) to (7);
- 4         Feed processed data into the SpectrumFM encoder to obtain the latent representation  $\mathbf{x}_{\text{latent}}^{(L)}$  according to equations (8) to (19);
- 5         Compute the classification loss for AMC, WTC, and SS tasks according to equations (26) to (27) or the AD task loss according to equation (28);
- 6         Update  $\Theta$  by using the classification loss or the AD task loss according to  $\Theta \leftarrow \Theta - \eta \nabla_{\Theta} \mathcal{L}$ ;
- 7     **end**
- 8 **end**
- 9 Return finetuned parameters  $\Theta$ ;

---

task-relevant labeled dataset. The primary goal of fine-tuning is to adjust a limited set of model parameters, enabling the model to effectively capture task-specific characteristics while preserving the general knowledge acquired during pre-training. The fine-tune framework for AMC, WTC, and SS tasks is shown in Fig. 2a. In particular, the input sequence is first



(a) The fine-tune framework for AMC, WTC, and SS tasks.



(b) The fine-tune framework for AD task.

Fig. 2: The fine-tune framework for AMC, WTC, SS, and AD tasks.

processed through the SpectrumFM encoders to generate a sequence of hidden states as described in equations (8) to (19). These hidden states are subsequently aggregated leveraging an LSTM network. Finally, the aggregated hidden state is passed through a linear layer, followed by a softmax function, to perform the classification task, given as

$$\hat{\mathbf{y}} = \text{softmax} \left( \text{LSTM} \left( \mathbf{x}_{\text{latent}}^{(L)} \right) \mathbf{W}_f + \mathbf{b}_f \right), \quad (26)$$

where  $\mathbf{W}_f \in \mathbb{R}^{d \times C}$  and  $\mathbf{b}_f \in \mathbb{R}^C$  are the weights and biases of the linear layer, respectively, and  $C$  is the number of classes. The cross-entropy loss is leveraged to fine-tune for the AMC, WTC, and SS tasks, given as

$$\mathcal{L}_{\text{classification}} = - \sum_{a=1}^C y_a \log(\hat{y}_a). \quad (27)$$

The fine-tune framework for AD task is shown in Fig. 2b. The input sequence is first processed through the SpectrumFM encoders to obtain a series of hidden states (as described in equations (8) to (19)). Contrary to the methodology employed in classification tasks, wherein hidden states undergo aggregation via an LSTM network, the proposed framework directly feeds the hidden states into a decoder layer to generate a reconstructed signal, given as

$$\hat{\mathbf{x}} = \tanh \left( \mathbf{x}_{\text{latent}}^{(L)} \mathbf{W}_a + \mathbf{b}_a \right), \quad (28)$$

where  $\mathbf{W}_a \in \mathbb{R}^{d \times 2}$  and  $\mathbf{b}_a \in \mathbb{R}^2$  are the weights and biases of the decoder layer, respectively, and  $\tanh(\cdot)$  is the tanh activation function. The reconstructed signal is then compared with the original input signal to compute the MSE reconstruction loss. The MSE loss serves as the criterion for distinguishing normal from anomalous signals. A low reconstruction loss indicates that the signal is normal, whereas a high loss suggests the presence of an anomaly, given as

$$\mathcal{L}_{AD} = \frac{1}{N} \sum_{p=1}^N (\hat{x}_p - x_p)^2. \quad (29)$$

The fine-tuning algorithm is summarized in Algorithm 2.

#### IV. EXPERIMENTS

In this section, we first present the experimental settings, followed by the experiments on four downstream spectrum management tasks, including AMC, WTC, SS, and AD.

##### A. Experimental Settings

The SpectrumFM is pre-trained on a setup comprising four NVIDIA RTX 4090 GPUs, utilizing PyTorch and DeepSpeed for efficient training. The hyperparameters for SpectrumFM are as follows. The mask ratio  $r$  is set to 15%, the number of signal symbols is set to 128, the number of attention heads  $H$  is set to 4, the latent dimension  $d$  is set to 256, the feedforward dimension  $d_{\text{feed}}$  is set to 512, and the number of SpectrumFM encoder layers  $L$  is set to 16. The pre-training phase consists of 10 epochs with a batch size of 256 and a learning rate of 0.001. The AdamW optimizer is employed for optimization, and early stopping is utilized to prevent overfitting. During the fine-tuning stage, the same learning rate of 0.001 and the AdamW optimizer are used to further adapt the model to specific downstream tasks.

##### B. Automatic Modulation Classification Task

1) *Dataset*: We leverage the RML2016 datasets <sup>3</sup> for AMC task. The RML2016 datasets, including RML2016.10A, RML2016.10B, and RML2016.04C, are benchmark datasets widely used for AMC task in wireless communications. RML2016.10A contains 11 modulation types under various SNR conditions, providing a foundational testbed for evaluating AMC task. RML2016.10B emphasizes real-world RF signals captured in complex propagation environments, offering a more challenging scenario. RML2016.04C further extends the challenges by incorporating effects such as multipath fading and Doppler shifts, rigorously testing the robustness of classifiers in dynamic channel conditions.

2) *Baselines*: We leverage 10 state-of-the-art baseline models for the AMC task. The outlines of the models are as follows.

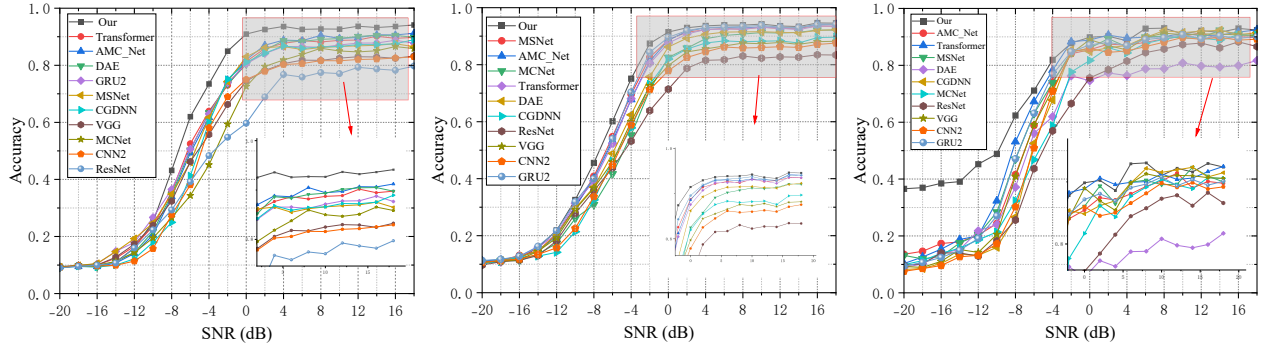
- AMC\_Net [17] employs a frequency-domain denoising module and a multi-scale feature extraction mechanism, leveraging attention operations to enhance modulation classification accuracy.
- Transformer [35] leverages the self-attention mechanism to extract features from the input signal.
- MSNet [40] leverages a multi-scale feature extraction and fusion mechanism to classify the modulation schemes.
- CGDNN [41] composes of a shallow convolutional network, a gated recurrent unit, and a deep neural network, for robust automatic modulation recognition.
- DAE [42] is an LSTM denoising auto-encoder framework that efficiently extracts robust features from noisy radio signals for the classification of communication technologies and modulation schemes.
- MCNet [43] employs specialized convolutional blocks with asymmetric kernels to concurrently capture spatio-temporal signal correlations, enhancing classification accuracy and efficiency.
- ResNet [44] is a residual network, a widely used deep learning model.
- VGG [39] is a 1D CNN network that adapt the VGG architecture principles.
- CNN2 [39] is a CNN classifier model for classifying modulation schemes according to their families.
- GRU2 [45] is a two layers of the GRU classifier model.

3) *Overall Performance*: To evaluate the overall performance of our proposed method for the AMC task, we conduct extensive experiments on three datasets, namely RML2016.10A, RML2016.10B, and RML2016.04C. The results are summarized in TABLE II, which presents the precision, recall, and F1-score for various models. The results underscore the superior capability of our model in the AMC task, achieving notable improvements in precision, recall, and F1-score over other baseline models. Specifically, our model attains F1-scores of 66.20% on RML2016.10A, 65.93% on RML2016.10B, and 73.46% on RML2016.04C, outperforming baselines like Transformer and AMC\_Net by 2.65-9.61 percentage points. Notably, it demonstrates robust pre-

<sup>3</sup><https://www.deepsig.ai/datasets/>

TABLE II: The Overall Performance in the AMC Task.

Dataset	RML2016.10A			RML2016.10B			RML2016.04C		
Model	Precision (%)	Recall (%)	F1 (%)	Precision (%)	Recall (%)	F1 (%)	Precision (%)	Recall (%)	F1 (%)
ResNet	54.27	50.04	48.94	57.16	54.88	52.80	64.43	55.97	57.04
MCNet	60.19	53.52	54.79	60.78	59.22	59.61	65.97	59.57	61.11
VGG	67.99	54.72	54.06	71.04	58.65	59.31	<b>74.80</b>	61.88	63.85
CNN2	68.67	53.25	55.32	64.61	57.14	57.27	74.69	59.45	62.33
GRU2	68.19	58.80	60.22	66.15	<u>64.11</u>	63.97	71.46	63.13	64.81
DAE	69.96	58.97	60.72	64.88	61.46	61.17	53.61	55.91	53.85
CGDNN	<u>73.03</u>	56.57	59.36	64.23	58.26	59.53	75.21	60.34	63.37
Transformer	68.26	<u>59.27</u>	61.08	68.75	63.10	63.28	71.31	<u>65.41</u>	66.70
MSNet	69.41	58.33	60.60	65.29	63.49	63.50	71.02	63.66	65.36
AMC_Net	71.41	59.10	<u>61.11</u>	<u>69.25</u>	63.38	<u>64.05</u>	68.03	63.01	64.35
Our	<b>75.29</b>	<b>63.72</b>	<b>66.20</b>	<b>70.07</b>	<b>65.35</b>	<b>65.93</b>	73.93	<b>73.37</b>	<b>73.46</b>



(a) The accuracy of models on different SNR conditions on RML2016.10A dataset. (b) The accuracy of models on different SNR conditions on RML2016.10B dataset. (c) The accuracy of models on different SNR conditions on RML2016.04C dataset.

Fig. 3: The accuracy of models on different SNR conditions in the AMC task.

cision (75.29% on RML2016.10A) and recall (73.37% on RML2016.04C), addressing challenges in class imbalance.

4) *The Performance on Various SNR Conditions*: To evaluate the robustness of our proposed method, its performance is assessed and contrasted with several baseline models across different SNR values, as illustrated in Fig. 3. The findings highlight the exceptional capability of our method across varying SNR conditions on three distinct datasets, namely, RML2016.10A, RML2016.10B, and RML2016.04C. Particularly, on the RML2016.10A dataset (Fig. 3a), our method showcases a marked improvement in accuracy at low SNR levels (-10 to 0 dB), significantly outperforming all other models. The trend continues on the RML2016.10B dataset (Fig. 3b), where our method maintains its superior performance across the entire SNR range, demonstrating enhanced reliability. Furthermore, the robustness of our method is particularly evident on the RML2016.04C dataset (Fig. 3c), our method not only consistently outperforms other models but also shows a particularly significant advantage under challenging low SNR conditions (-10 to -5 dB). These results collectively emphasize the efficacy of our proposed method in achieving high accuracy across diverse SNR conditions, underscoring its superior performance and resilience in various communication environments.

The confusion matrices for our proposed model and the two most competitive baseline models, namely AMC\_Net and Transformer under SNR conditions of -4 dB, 0 dB, and 4 dB are shown in Fig. 4, revealing interesting insights into their classification performance. At low SNR (-4 dB), all

three models exhibit relatively poor classification performance, with significant confusion between modulation types such as AM-DSB, 16-QAM, and QPSK. However, it is clear that the proposed method achieves better diagonal clarity and fewer off-diagonal errors compared to AMC\_Net and Transformer, indicating stronger noise robustness. As the SNR increases to 0 dB, the classification performance of all methods improves significantly. Notably, the confusion matrices of the Transformer and the proposed method show a clear diagonal trend with reduced misclassification. The proposed method consistently outperforms the other two, with higher correct classification counts and fewer false predictions, especially for easily confused categories such as QPSK and 64-QAM. At high SNR (4 dB), the performance gap becomes more evident. The proposed method achieves near-perfect classification accuracy, with almost all samples correctly classified and the confusion matrix showing a clean diagonal structure. In comparison, AMC\_Net and Transformer still exhibit sporadic misclassification, particularly in closely related classes such as 64-QAM and 8-PSK.

The t-SNE visualizations of the RML2016.10A dataset under 0 dB SNR condition for our proposed model, AMC\_Net and Transformer is presented in Fig. 5. The t-SNE visualizations reveal notable clustering overlaps for the AMC\_Net model, specifically between 8-PSK and 64-QAM, 16-QAM and QPSK, WBFM and AM-DSB, as well as WBFM and GFSK. The overlaps indicate difficulties in distinguishing the modulation types using AMC\_Net. Similarly, the Transformer model exhibits significant overlap between 16-QAM

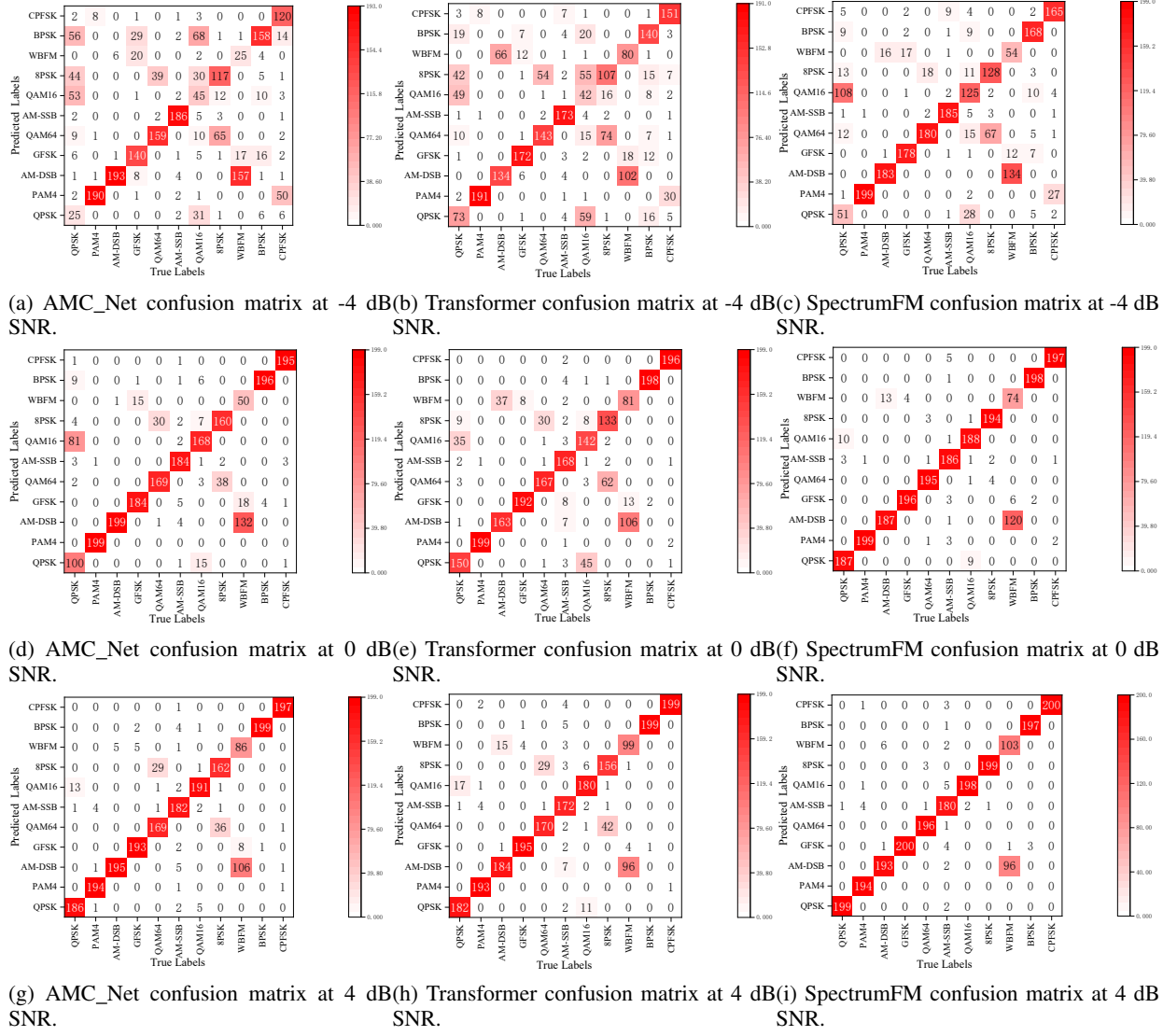
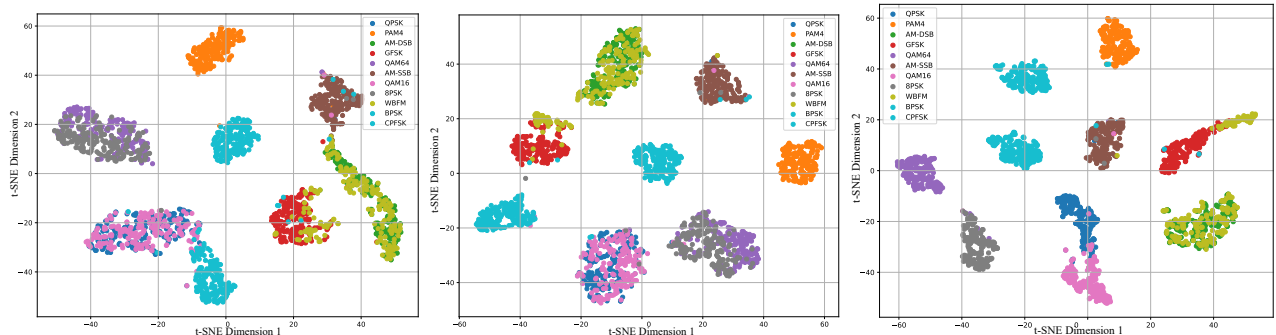
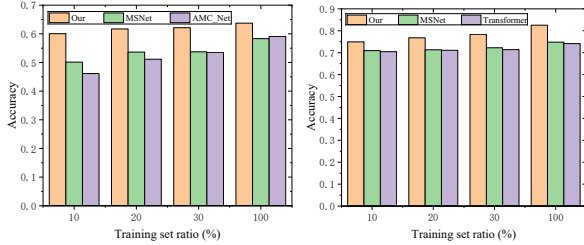


Fig. 4: The confusion matrices for the AMC\_Net, Transformer, and our proposed model under SNR conditions of -4 dB, 0 dB, and 4 dB.



(a) The t-SNE visualizations of the RML2016.10A dataset for AMC\_Net. (b) The t-SNE visualizations of the RML2016.10A dataset for Transformer. (c) The t-SNE visualizations of the RML2016.10A dataset for our model.

Fig. 5: The t-SNE visualizations of the RML2016.10A dataset under 0 dB SNR condition for our proposed model and two most competitive baseline models.



(a) Performance in few-shot conditions on RML2016.10A conditions (b) Performance in few-shot conditions on TechRec dataset.

Fig. 6: Performance in few-shot conditions.

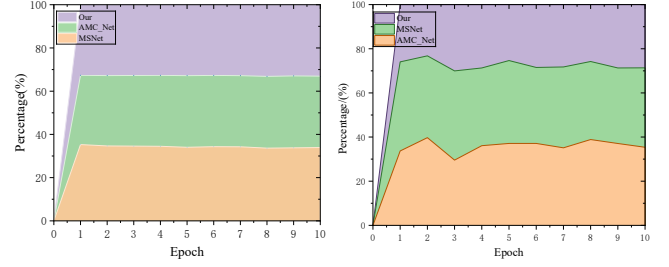
and QPSK, 8-PSK and 64-QAM, as well as WBFM and AM-DSB, suggesting similar challenges in classification accuracy for these pairs. In contrast, our proposed method demonstrates clear boundaries between most modulation classes, with the exception of some overlap between WBFM and AM-DSB. It indicates a higher discriminative capability for our model across various modulation types, thereby showcasing its superior performance compared to the baseline models.

5) *Performance in Few-shot Conditions*: The bar chart in Fig. 6a illustrates the classification accuracy of our method, MSNet, and AMC\_Net under different training set ratios (10%, 20%, 30%, and 100%). The vertical axis represents accuracy, while the horizontal axis denotes the proportion of the training set used for model training. From the results, it is evident that our proposed method consistently outperforms MSNet and AMC\_Net across all training set ratios. Notably, a key observation from the results is that as the training data ratio decreases, the accuracy of MSNet and AMC\_Net drops significantly, whereas our proposed method remains remarkably stable. Even when trained with only 10% of the dataset, our model achieves an accuracy comparable to MSNet and AMC\_Net trained on 100% of the data. The results highlight the strong few-shot learning capability of our method.

6) *Learning Efficiency*: To evaluate the learning efficiency of our method, the stacked percentage area chart in Fig. 7a illustrates the accuracy trends of three models, including our method, MSNet, and AMC\_Net, over ten training epochs. The vertical axis represents accuracy in percentage terms, while the horizontal axis denotes the number of epochs. A key observation from the figure is that our proposed method consistently occupies the largest area in the chart, indicating superior accuracy across all epochs. Furthermore, our method reaches a high accuracy level within the first few epochs, whereas MSNet and AMC\_Net require more epochs to stabilize. The results highlight the exceptional learning efficiency of our model.

### C. Wireless Technology Classification Task

1) *Dataset*: As detailed in Section III-A, the TechRec dataset comprises data captured from various locations including Merelbeke, iGent, and Rabot, which are utilized for pre-training our model. Meanwhile, data collected from the remaining sites, including UZ, Reep, and Gentbrugge, are re-



(a) The accuracy curve on RML2016.10A dataset. (b) The accuracy curve on TechRec dataset.

Fig. 7: The accuracy curve over epochs.

TABLE III: Comparison of Precision, Recall and F1-score in the WTC Task.

Models	Precision	Recall	F1 Score
ResNet	0.6723	0.6950	0.6764
VGG	0.7542	0.7404	0.7356
CNN2	0.7851	0.7509	0.7407
AMC_Net	0.6492	0.6472	0.6405
DAE	0.6826	0.6735	0.6487
CGDNN	0.7815	0.7488	0.7397
MCNet	0.7210	0.7320	0.7116
GRU2	0.7286	0.7429	0.7225
MSNet	0.7696	0.7546	0.7481
Transformer	0.7617	0.7463	0.7415
Our	<b>0.8270</b>	<b>0.8253</b>	<b>0.8226</b>

served for fine-tuning and testing, ensuring a robust evaluation of our model performance across different environments.

2) *Baselines*: We leverage AMC\_Net, Transformer, MSNet, CGDNN, DAE, MCNet, ResNet, VGG, CNN2 and GRU2 described in Section IV-B2 as baseline models.

3) *Performance Comparison*: The experimental results presented in TABLE III demonstrate the superior performance of our proposed model compared to existing methods in the WTC task. Specifically, our model achieves the highest precision (0.8270), recall (0.8253), and F1-score (0.8226), significantly outperforming the baseline methods. Notably, compared to well-established architectures such as ResNet and VGG, our model exhibits substantial improvements, particularly in Recall and F1-score, indicating its enhanced ability to correctly classify instances while maintaining robustness against misclassification.

The accuracy of various models under different SNR conditions is illustrated in Fig. 8. The figure demonstrates that our proposed method achieves superior performance across a wide range of SNR levels. Specifically, our method consistently outperforms other methods. At SNR levels from -15 dB to 0 dB, our method exhibits a higher accuracy rate compared to the other models. As the SNR increases beyond 0 dB, all methods show improved accuracy, but our method maintains a notable lead. The robust performance underscores the effectiveness of our method in both challenging and favorable SNR conditions.

As evidenced in the percentage area stacked plot in Fig. 7b, our proposed model not only converges more rapidly but also achieves a higher accuracy rate across all epochs, demonstrating its superior learning efficiency compared to AMC\_Net and MSNet.

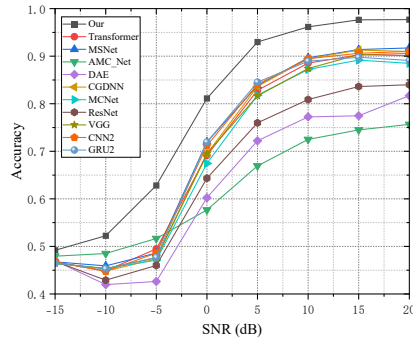


Fig. 8: The accuracy of models on different SNR conditions on the TechRec dataset.

#### D. Spectrum Sensing Task

1) *Dataset*: The RML2018.01A dataset is a widely used benchmark for AMC. It consists of IQ signal samples representing various digital and analog modulation schemes under different SNR conditions. In this study, pure noise is added to the dataset to enhance its applicability for spectrum sensing task.

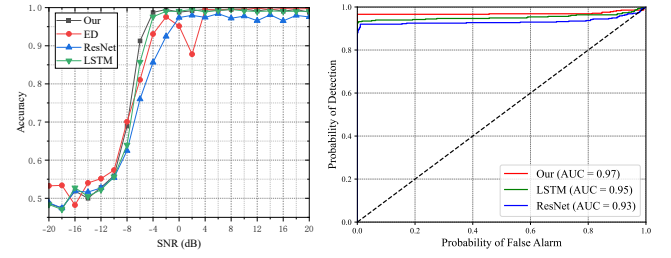
2) *Baselines*: We leverage energy detection (ED), along with the ResNet and LSTM models mentioned in Section IV-B2, as baseline methods. Energy detection is a fundamental spectrum sensing method that determines the presence or absence of a signal by comparing the received signal energy to a predefined threshold. Due to its low computational complexity and independence from prior signal knowledge, it serves as a widely used benchmark in spectrum sensing research.

3) *Performance Comparison*: Fig. 9a illustrates the performance of different spectrum sensing methods at various SNR levels. All methodologies exhibit poor performance when the SNR is between -10 dB and -4 dB. However, within the range of SNR from -10 dB to 0 dB, our proposed method demonstrates a higher accuracy rate. Beyond 0 dB, all methodologies achieve nearly perfect sensing accuracy.

Fig. 9b shows the receiver operating characteristic (ROC) curve of various spectrum sensing method at -4 dB SNR level. It highlights that our method achieves an AUC of 0.97 at -4 dB SNR, surpassing both LSTM and ResNet, demonstrating its superior accuracy in signal detection. At the same false alarm rate, our method also exhibits better detection performance, further underscoring its effectiveness in the SS task.

#### E. Anomaly Detection Task

1) *Datasets*: The dataset used for AD task is collected over a two-day period using an over-the-air (OTA) platform, shown in Fig. 10, which is designed to simulate real-world wireless communication environments. A ceyear 1435B-V RF signal generator is employed to transmit the PU signal, which is modulated using QPSK with a carrier frequency of 2.9 GHz and a bandwidth of 20 MHz. To introduce interference, a ceyear 1465B-V RF signal generator is positioned approximately two meters away, generating abnormal signals intended to disrupt the normal transmission. A SAM 60 MK2 receiver, placed ten



(a) Sensing accuracy of our model and baseline models at trum sensing method at -4 dB various SNR level.

Fig. 9: Performance comparison of our model and baseline methods in the SS task.

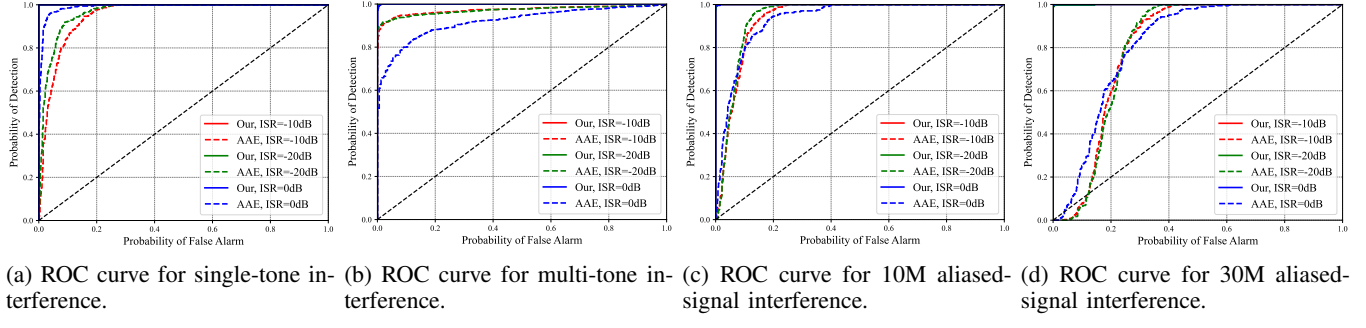


Fig. 10: The data acquisition and SpectrumFM deployment platform.

meters from both transmitters, is used to capture the received signals. To replicate realistic interference scenarios, three types of anomalies are introduced. The single-tone interference consisted of a sinusoidal signal sweeping across 2.89 GHz to 2.91 GHz, while the multi-tone interference involved multiple sinusoids sweeping within the same frequency range. The aliased-signal interference is created by generating random signals with bandwidths of 10 MHz and 30 MHz, appearing at 2.885 GHz to 2.915 GHz, thereby causing aliasing effects with the normal QPSK-modulated signal. To further increase the complexity of the aliased interference, these random signals are also QPSK-modulated, making them more challenging to distinguish from the normal transmission.

2) *Baseline*: We leverage adversarial autoencoder (AAE) [46] as the baseline model for AD task. The AAE is a generative model that integrates an autoencoder with a discriminator to enforce a specific feature distribution in the latent space. In AAE, the autoencoder consists of an encoder-decoder pair, where the encoder maps input data to a latent representation, and the decoder reconstructs the original input from this representation. Furthermore, a discriminator is employed to guide the encoder in shaping the latent space to follow a predefined distribution, such as a Gaussian or other structured priors.

3) *Performance Comparison*: Fig. 11 presents the ROC curves for four types of interference under varying interference-to-signal ratios (ISR), comparing the performance



(a) ROC curve for single-tone interference. (b) ROC curve for multi-tone interference. (c) ROC curve for 10MHz aliased-signal interference. (d) ROC curve for 30MHz aliased-signal interference.

Fig. 11: Comparison of anomaly detection performance among various types of interference.

of our proposed method with the AAE. Across all scenarios, our method consistently achieves an AUC of 1.0 at -20 dB and -10 dB ISR, showcasing an excellent balance between detection probability and false alarm rate. Even at 0 dB ISR, our method maintains near-optimal performance, with AUC values significantly outperforming those of AAE, indicating superior robustness and detection capability. Moreover, in the case of aliased-signal interference, the baseline AAE method exhibits a significant decline in performance. The aliased-signal interference is particularly challenging to detect due to its close resemblance to normal signals. Specifically, for 30 MHz aliased-signal interference at 0 dB ISR, the AAE AUC decreases to 0.84, markedly lower than its performance on other less complex interference types. In contrast, our proposed method consistently achieves an AUC of 1.0 across all ISR for both 10 MHz and 30 MHz aliased-signal interferences. All the findings underscore the robustness, high detection rate, and strong generalization ability of our model.

#### F. Discussion

In summary, the superior performance of our model across AMC, WTC, SS, and AD tasks can be attributed to its capacity to effectively learn and generalize spectral features through large-scale pre-training. By exploiting MHSA and convolutional modules, the model captures fine-grained signal characteristics and learns universal spectral patterns, enabling it to perform effectively in diverse, unseen environments. Large-scale pre-training facilitates the development of transferable representations, which enhances the model generalization ability and makes it highly effective even under low SNR or noisy conditions. Additionally, the leveraging of masked reconstruction tasks during pre-training bolsters the model robustness to signal distortions and interference, fostering enhanced resilience in challenging real-world conditions. The next-slot signal prediction task, in particular, improves the model capacity to anticipate future signal behaviors based on both current and past information, thereby enabling it to navigate dynamic spectrum environments with greater accuracy. These tasks, collectively, significantly augment the model predictive power and robustness, making it particularly well-suited for complex and unpredictable spectrum scenarios.

These advancements offer substantial benefits for wireless communication systems. The improved modulation recognition ensures efficient signal classification, which is critical

for adaptive transmission strategies. Technology classification, in turn, enhances interoperability in complex spectrum environments. Furthermore, spectrum sensing facilitates dynamic spectrum access, while anomaly detection strengthens security by mitigating interference and detecting unauthorized transmissions.

#### V. CONCLUSION

In this paper, we introduced SpectrumFM, a foundation model designed for spectrum management, representing a novel paradigm in this field. To support its training, a diverse spectrum dataset was collected and processed from multiple sources, including publicly available open-source datasets and self-collected real-world data. To pre-train SpectrumFM, an encoder architecture exploiting CNNs with MHSA mechanisms was designed to enhance both high-level and fine-grained feature extraction as well as representation learning. Additionally, two novel self-supervised tasks, namely masked reconstruction and next-slot signal prediction, were proposed to enable the model to learn generalizable and foundational spectrum representations. Furthermore, a parameter-efficient fine-tuning strategy was proposed to enable SpectrumFM to effectively adapt to diverse downstream tasks. Extensive experiments conducted across four key spectrum management tasks, including AMC, WTC, SS, and AD, highlight its remarkable efficiency and performance gains over state-of-the-art methods. Specifically, SpectrumFM achieves up to 12.1% accuracy improvement in AMC, 9.3% in WTC, an AUC of 0.97 in SS at -4 dB SNR, and an AUC gain exceeding 10% in AD, underscoring its superior capability in spectrum management. For future research, we will focus on expanding the data scale and model size to improve performance and generalization. Additionally, we believe SpectrumFM can also facilitate dynamic spectrum access, spectrum resource allocation, and secure spectrum sharing.

#### REFERENCES

- [1] J. Sun, J. Chen, G. Ding, F. Lin, and Y. Song, "Spectrum recommendation in cognitive Internet of Things: A knowledge-graph-based framework," *IEEE Trans. Cognit. Commun. Netw.*, vol. 10, no. 1, pp. 21–34, 2024.
- [2] A. Gao, Q. Wang, Y. Wang, C. Du, Y. Hu, W. Liang, and S. X. Ng, "Attention enhanced multi-agent reinforcement learning for cooperative spectrum sensing in cognitive radio networks," *IEEE Trans. Veh. Technol.*, vol. 73, no. 7, pp. 10464–10477, 2024.

[3] J. Li, L. Yang, Q. Wu, X. Lei, F. Zhou, F. Shu, X. Mu, Y. Liu, and P. Fan, "Active RIS-aided noma-enabled space-air-ground integrated networks with cognitive radio," *IEEE J. Sel. Areas Commun.*, vol. 43, no. 1, pp. 314–333, 2025.

[4] Y. Xu, Y. Li, and T. Q. S. Quek, "RIS-enhanced cognitive integrated sensing and communication: Joint beamforming and spectrum sensing," *IEEE J. Sel. Areas Commun.*, vol. 43, no. 3, pp. 795–810, 2025.

[5] H. Ji, T. Zhang, X. Qiao, H. Wu, and G. Gui, "TFAM-AAE-UK: A dual-metric spectrum anomaly detection algorithm," *IEEE Commun. Lett.*, vol. 28, no. 11, pp. 2638–2642, 2024.

[6] Y. Qu, H. Dai, H. Wang, C. Dong, F. Wu, S. Guo, and Q. Wu, "Service provisioning for UAV-enabled mobile edge computing," *IEEE J. Sel. Areas Commun.*, vol. 39, no. 11, pp. 3287–3305, 2021.

[7] J. Chamberlain, D. Starobinski, and J. T. Johnson, "Facilitating spectrum sharing with passive satellite incumbents," *IEEE J. Sel. Areas Commun.*, vol. 42, no. 12, pp. 3719–3733, 2024.

[8] Z. Huang, S. Zhong, P. Zhou, S. Gao, M. Zitnik, and L. Lin, "A causality-aware paradigm for evaluating creativity of multimodal large language models," *IEEE Trans. Pattern Anal. Mach. Intell.*, vol. 47, no. 5, pp. 3830–3846, 2025.

[9] S. Song, X. Li, S. Li, S. Zhao, J. Yu, J. Ma, X. Mao, W. Zhang, and M. Wang, "How to bridge the gap between modalities: Survey on multimodal large language model," *IEEE Trans. Knowl. Data Eng.*, 2025, to be published.

[10] D. Hong, B. Zhang, X. Li, Y. Li, C. Li, J. Yao, N. Yokoya, H. Li, P. Ghamisi, X. Jia, A. Plaza, P. Gamba, J. A. Benediktsson, and J. Chanussot, "SpectralGPT: Spectral remote sensing foundation model," *IEEE Trans. Pattern Anal. Mach. Intell.*, vol. 46, no. 8, pp. 5227–5244, 2024.

[11] T. Yang, P. Zhang, M. Zheng, Y. Shi, L. Jing, J. Huang, and N. Li, "WirelessGPT: A generative pre-trained multi-task learning framework for wireless communication," 2025. [Online]. Available: <https://arxiv.org/abs/2502.06877>

[12] H. Xing, X. Zhang, S. Chang, J. Ren, Z. Zhang, J. Xu, and S. Cui, "Joint signal detection and automatic modulation classification via deep learning," *IEEE Trans. Wireless Commun.*, vol. 23, no. 11, pp. 17129–17142, 2024.

[13] T. J. O'Shea, J. Corgan, and T. C. Clancy, "Convolutional radio modulation recognition networks," in *Int. Conf. Eng. Appl. Neural Netw.*, 2016, pp. 213–226.

[14] S. Huang, R. Dai, J. Huang, Y. Yao, Y. Gao, F. Ning, and Z. Feng, "Automatic modulation classification using gated recurrent residual network," *IEEE Internet Things J.*, vol. 7, no. 8, pp. 7795–7807, 2020.

[15] Z. Liang, M. Tao, J. Xie, X. Yang, and L. Wang, "A radio signal recognition approach based on complex-valued CNN and self-attention mechanism," *IEEE Trans. Cognit. Commun. Netw.*, vol. 8, no. 3, pp. 1358–1373, 2022.

[16] H. Zhang, F. Zhou, Q. Wu, and N. Al-Dhahir, "Sswsrnet: A semi-supervised few-shot learning framework for wireless signal recognition," *IEEE Trans. Commun.*, vol. 72, no. 9, pp. 5823–5836, 2024.

[17] J. Zhang, T. Wang, Z. Feng, and S. Yang, "AMC-Net: An effective network for automatic modulation classification," in *IEEE Int. Conf. Acoust. Speech Signal Process.*, 2023, pp. 1–5.

[18] M. Du, J. Pan, and D. Bi, "A contrastive learner for automatic modulation classification," *IEEE Trans. Wireless Commun.*, 2025, to be published.

[19] J. Fontaine, E. Fonseca, A. Shahid, M. Kist, L. A. DaSilva, I. Moerman, and E. De Poorter, "Towards low-complexity wireless technology classification across multiple environments," *Ad Hoc Netw.*, vol. 91, p. 101881, 2019.

[20] L. Yuan, H. Zhang, M. Xu, F. Zhou, and Q. Wu, "A multiscale CNN framework for wireless technique classification in internet of things," *IEEE Internet Things J.*, vol. 9, no. 12, pp. 10366–10367, 2022.

[21] M. Girmay, V. Maglogiannis, D. Naudts, M. Aslam, A. Shahid, and I. Moerman, "Technology recognition and traffic characterization for wireless technologies in ITS band," *Veh. Commun.*, vol. 39, pp. 1–15, 2023.

[22] Y. Peng, Y. Zhang, H. Huang, Y. Wang, P. Liu, Y. Lin, and G. Gui, "Low-complexity wireless technique classification with multifeature fusion broad learning network," *IEEE Internet Things J.*, vol. 11, no. 21, pp. 34434–34442, 2024.

[23] C. Vlădeanu, O. M. K. Al-Dulaimi, A. Martian, and D. C. Popescu, "Average energy detection with adaptive threshold for spectrum sensing in cognitive radio systems," *IEEE Trans. Veh. Technol.*, vol. 73, no. 11, pp. 17222–17230, 2024.

[24] M. U. Muzaffar and R. Sharqi, "A review of spectrum sensing in modern cognitive radio networks," *Telecommu. Syst.*, vol. 85, no. 2, pp. 347–363, 2024.

[25] P. Pawelczak, K. Nolan, L. Doyle, S. W. Oh, and D. Cabric, "Cognitive radio: Ten years of experimentation and development," *IEEE Commun. Mag.*, vol. 49, no. 3, pp. 90–100, 2011.

[26] J. Gao, X. Yi, C. Zhong, X. Chen, and Z. Zhang, "Deep learning for spectrum sensing," *IEEE Wireless Commun. Lett.*, vol. 8, no. 6, pp. 1727–1730, 2019.

[27] W. Zhang, Y. Wang, X. Chen, Z. Cai, and Z. Tian, "Spectrum transformer: An attention-based wideband spectrum detector," *IEEE Trans. Wireless Commun.*, vol. 23, no. 9, pp. 12343–12353, 2024.

[28] X. Hao, S. Yang, R. Liu, Z. Feng, T. Peng, and B. Huang, "VSLM: Virtual signal large model for few-shot wideband signal detection and recognition," *IEEE Trans. Wireless Commun.*, vol. 24, no. 2, pp. 909–925, 2025.

[29] P. Qi, T. Jiang, J. Xu, J. He, S. Zheng, and Z. Li, "Unsupervised spectrum anomaly detection with distillation and memory enhanced autoencoders," *IEEE Internet Things J.*, vol. 11, no. 24, pp. 39361–39374, 2024.

[30] Y. Kang, H. Wu, Z. Zhao, Y. Li, and J. Meng, "DL-based anomaly detection at the physical-layer of cognitive radio by deep support vector data description," *IEEE Trans. Cognit. Commun. Netw.*, vol. 8, no. 4, pp. 1689–1705, 2022.

[31] H. Zhang, Z. Song, J. Yang, and Y. Gao, "Adversarial autoencoder empowered joint anomaly detection and signal reconstruction from sub-Nyquist samples," *IEEE Trans. Cognit. Commun. Netw.*, vol. 9, no. 3, pp. 618–628, 2023.

[32] M. Fang, R. Ding, F. Zhou, and Q. Wu, "A simultaneous spectrum sensing and anomaly detection deep learning framework for dynamic spectrum sharing networks," in *Int. Conf. Commun. Image Signal Process.*, 2024, pp. 107–111.

[33] M. Awais, M. Naseer, S. Khan, R. M. Anwer, H. Cholakkal, M. Shah, M.-H. Yang, and F. S. Khan, "Foundation models defining a new era in vision: a survey and outlook," *IEEE Trans. Pattern Anal. Mach. Intell.*, 2025, to be published.

[34] C. Liu, W. Wu, S. Wu, L. Yuan, R. Ding, F. Zhou, and Q. Wu, "Social-enhanced explainable recommendation with knowledge graph," *IEEE Trans. Knowl. Data Eng.*, vol. 36, no. 2, pp. 840–853, 2024.

[35] A. Vaswani, N. Shazeer, N. Parmar, J. Uszkoreit, L. Jones, A. N. Gomez, Ł. Kaiser, and I. Polosukhin, "Attention is all you need," *Int. Conf. Neural Inf. Process. Syst.*, vol. 30, 2017.

[36] J. Devlin, M.-W. Chang, K. Lee, and K. Toutanova, "BERT: Pre-training of deep bidirectional transformers for language understanding," in *Conf. North Am. Chapter Assoc. Comput. Linguistics*, 2019, pp. 4171–4186.

[37] W.-N. Hsu, B. Bolte, Y.-H. H. Tsai, K. Lakhotia, R. Salakhutdinov, and A. Mohamed, "Hubert: Self-supervised speech representation learning by masked prediction of hidden units," *IEEE/ACM Trans. Audio, Speech Lang. Process.*, vol. 29, pp. 3451–3460, 2021.

[38] T. Chen, S. Saxena, L. Li, T.-Y. Lin, D. J. Fleet, and G. Hinton, "A unified sequence interface for vision tasks," in *Int. Conf. Neural Inf. Process. Syst.*, 2022, pp. 31333–31346.

[39] T. J. O'Shea, T. Roy, and T. C. Clancy, "Over-the-air deep learning based radio signal classification," *IEEE J. Sel. Topics Signal Process.*, vol. 12, no. 1, pp. 168–179, 2018.

[40] H. Zhang, F. Zhou, Q. Wu, W. Wu, and R. Q. Hu, "A novel automatic modulation classification scheme based on multi-scale networks," *IEEE Trans. Cognit. Commun. Netw.*, vol. 8, no. 1, pp. 97–110, 2022.

[41] J. N. Njoku, M. E. Morocho-Cayamela, and W. Lim, "CGDNET: Efficient hybrid deep learning model for robust automatic modulation recognition," *IEEE Netw. Lett.*, vol. 3, no. 2, pp. 47–51, 2021.

[42] Z. Ke and H. Vikalo, "Real-time radio technology and modulation classification via an LSTM auto-encoder," *IEEE Trans. Wireless Commun.*, vol. 21, no. 1, pp. 370–382, 2022.

[43] T. Huynh-The, C.-H. Hua, Q.-V. Pham, and D.-S. Kim, "MCNet: An efficient CNN architecture for robust automatic modulation classification," *IEEE Commun. Lett.*, vol. 24, no. 4, pp. 811–815, 2020.

[44] X. Liu, D. Yang, and A. E. Gamal, "Deep neural network architectures for modulation classification," in *Asilomar Conf. Signals, Syst., Comput.*, 2017, pp. 915–919.

[45] D. Hong, Z. Zhang, and X. Xu, "Automatic modulation classification using recurrent neural networks," in *IEEE Int. Conf. Comput. Commun.*, 2017, pp. 695–700.

[46] H. Zhang, Z. Song, J. Yang, and Y. Gao, "Adversarial autoencoder empowered joint anomaly detection and signal reconstruction from sub-Nyquist samples," *IEEE Trans. Cognit. Commun. Netw.*, vol. 9, no. 3, pp. 618–628, 2023.